

transfer cross section cannot be excluded; however, there is no reason to expect it on the basis of effective-range scattering theory.

<sup>37</sup>C. L. Chen, *Phys. Rev.* **131**, 2550 (1963).

<sup>38</sup>As in the case of neon, a fit to our cross section

cannot be obtained over an extended energy range by adjusting only the scattering length. However, the higher-order term is relatively unimportant at low energy.

<sup>39</sup>A tabulation of the measured cross sections is available on request.

PHYSICAL REVIEW

VOLUME 178, NUMBER 1

5 FEBRUARY 1969

## Ionization and Attachment in O<sub>2</sub> and Airlike N<sub>2</sub>: O<sub>2</sub> Mixtures Irradiated by 1.5-MeV Electrons\*

M. N. Hirsh, P. N. Eisner, and J. A. Slevin<sup>†</sup>  
*The G. C. Dewey Corporation, New York, New York 10016*  
(Received 1 August 1968)

The production and removal of thermal electrons has been studied in O<sub>2</sub> and airlike N<sub>2</sub>: O<sub>2</sub> mixtures between 1 and 10 Torr during continuous and intermittent irradiation by 1.5-MeV electrons. The use of a large reaction chamber and a spatially uniform electron beam flux reduces diffusion losses two orders of magnitude below those in previous experiments, and permits direct measurements of electron attachment at correspondingly lower total gas pressures. The observed rate coefficients for three-body attachment of thermal electrons at 300°K are  $k_3(\text{O}_2) = (2.12 \pm 0.14) \times 10^{-30}$  cm<sup>6</sup>/sec and  $k_3(4\text{N}_2: \text{O}_2) = (1.10 \pm 0.07) \times 10^{-31}$  cm<sup>6</sup>/sec, both during irradiation and in the afterglow. The effective cross sections for ionization by 1.5-MeV electrons and all resulting secondaries are  $\sigma_e(\text{O}_2) = (2.83 \pm 0.7) \times 10^{-18}$  cm<sup>2</sup> and  $\sigma_e(4\text{N}_2: \text{O}_2) = (2.45 \pm 0.7) \times 10^{-18}$  cm<sup>2</sup>. These effective cross sections are larger than recently measured cross sections for primary ionization by a factor of  $3.0 \pm 0.8$  in both gases.

### I. INTRODUCTION

Charged particle production and loss mechanisms in atmospheric gases are being investigated in this laboratory under conditions relevant to the normal and the mildly perturbed ionosphere. This paper presents the results of measurements of ionization and electron attachment in O<sub>2</sub> and airlike N<sub>2</sub>: O<sub>2</sub> mixtures irradiated by 1.5-MeV electrons.

Many ionospheric phenomena are initiated by the impact of energetic particles on the upper atmosphere. These include natural events such as auroras, and man-made disturbances such as the blackout of electromagnetic communications following a high-altitude nuclear detonation. The fast particles produce excited atoms and molecules as well as electrons and positive ions. The subsequent behavior of these newly formed species is controlled by various reactions, many of them dependent on the distribution of excitation in the reactants.

Previous laboratory investigations of thermal-energy reactions of charged particles have utilized low-energy electron-swarm techniques,<sup>1,2</sup> irradiation by  $\gamma$  rays,<sup>3</sup> flowing afterglows<sup>4</sup> and the afterglows of microwave discharges,<sup>5-7</sup> and of intense pulses of relativistic electrons.<sup>8</sup> Each of these techniques produces a characteristic distribution of charged particles, excited states, and new chemical species. None, however, duplicates the

geophysically interesting situation of prolonged weak ionization by relativistic electrons. In particular, it is desirable to study electron-induced reactions both during irradiation and in the afterglow to evaluate the role of short-lived species created by the beam which may not persist into the afterglow. The technique employed in the present work is an attempt to reproduce the important features of the ionospheric situation in the laboratory and thus permit the direct evaluation of some of these effects.

### II. EXPERIMENTAL TECHNIQUES

The experiment is shown schematically in Fig. 1. Gas is contained in a stainless-steel chamber 1.2 m in diameter and 0.6 m long, closed at one end by a 0.012-cm-thick aluminum foil. A diffuse beam of 1.5-MeV electrons from the Van de Graaff accelerator traverses the foil window and irradiates the gas, producing secondary electrons, ions, and excited species in collisions with the neutral molecules. The resultant ionization is studied by means of resonant cavity measurements of the free-electron density. Mass spectrometry, optical spectrometry, and low-frequency plasma-impedance measurements are also available for diagnostics; results obtained with these other techniques will be described in future publications. A detailed

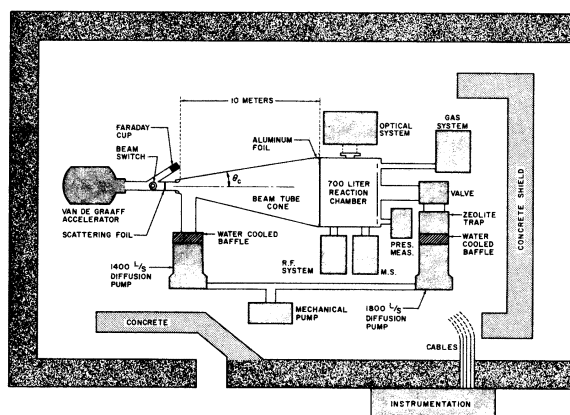


FIG. 1. Schematic diagram of experimental system. The optical and mass spectrometer (M. S.) systems were not employed for the work described in this paper.

description of the experimental equipment can be found elsewhere.<sup>9</sup>

At pressures below 10 Torr, 1.5-MeV electrons lose a negligible amount of their incident energy while traversing the gas. The spatial distribution of this monoenergetic flux is determined by multiple Coulomb scattering of the Van de Graaff electrons in a beryllium foil located 10 m in front of the cavity. The geometry is so chosen that the nearly uniform central 30% of the scattered beam fills the volume of the gas in the chamber; the ionization production term is thus constant over the gas volume to within 20%. Faraday-cup measurements of the beam flux in the chamber yield the calibration: 1  $\mu\text{A}$  from the accelerator corresponds to  $3.1 \times 10^{-5} \mu\text{A}/\text{cm}^2$  at the center of the chamber, and to an average flux over the entire gas volume of  $2.88 \times 10^{-5} \mu\text{A}/\text{cm}^2$ , accurate to within  $\pm 20\%$ .

Because of the small surface-to-volume ratio of the reaction chamber, particle-loss rates due to diffusion are about two orders of magnitude smaller at a given pressure than in apparatus of the size used in previous laboratory measurements.<sup>5-8</sup> This permits the study of intermolecular processes at lower pressures than can usually be accomplished in the laboratory. The quenching of beam-generated excited states by wall collisions is also significantly reduced.

Ultrahigh-vacuum techniques, including system bakeout at  $200^\circ\text{C}$ , and the use of high purity gases, minimize the contamination of the observed reactions by impurity processes. The pressure attained in the chamber prior to gas filling is in the range  $0.5$  to  $1.5 \times 10^{-8}$  Torr. With the system closed to the pumps, the rate of rise of pressure in the reaction chamber is on the order of  $5 \times 10^{-6}$  Torr/h.

The reaction chamber is a uhf cavity resonant in the  $\text{TE}_{011}$  mode at 390 MHz with a loaded  $Q$  of about 16 000. At low pressures, a uniform distribution of  $n_e$  electrons/ $\text{cm}^3$  throughout the gas increases the resonant frequency by an amount  $0.10n_e$  Hz.<sup>9</sup> Electron densities as small as  $10^4/$

$\text{cm}^3$ , corresponding to frequency shifts of 1 kHz, can be measured reproducibly. In general, the measured frequency shifts must be corrected for the electron spatial distribution and for electron-neutral molecule collisions.<sup>8</sup>

The density  $n_e$  of free electrons in a weakly ionized gas can be described by the general rate equation

$$\frac{\partial n_e}{\partial t} = P - \nu_L n_e \quad (1)$$

Here  $P$  is the instantaneous rate of production of electrons, and  $\nu_L$  is the effective electron removal frequency.  $\nu_L$  is in general a function of charged particle densities and their gradients, the internal and kinetic energies of the interacting species, and the pressure, temperature, and chemical composition of the gas.

During continuous irradiation by the electron beam, a steady-state distribution of charged and neutral excited species is established; this distribution is studied as a function of the beam flux, and of the pressure, temperature, and chemical composition of the gas. The density of beam electrons is sufficiently low ( $< 100/\text{cm}^3$ ) to avoid interference with the measurement of the density of the slower secondaries. The steady-state electron density  $n_{e0}$  is described by

$$P = \nu_{L0} n_{e0} \quad (2)$$

where  $\nu_{L0}$  is the loss frequency during continuous irradiation.

Alternatively, the beam can be pulsed on and off periodically, and time-resolved measurements made in the radiation afterglow. If free electrons are produced only by the impact of beam electrons, then in the afterglow  $P=0$ , and

$$\left(\frac{\partial n_e}{\partial t}\right)_{\text{afterglow}} = -\nu_L n_e(t) \quad (3)$$

### III. EXPERIMENTAL RESULTS

Electron-density measurements were made during both continuous and pulsed irradiation of  $\text{O}_2$  and airlike mixtures of oxygen and nitrogen ( $4\text{N}_2:\text{O}_2$ ) at  $300^\circ\text{K}$  and pressures between 0.7 and 10 Torr. Figure 2 shows typical measurements of  $n_{e0}$  in this pressure range as a function of the flux of beam electrons from the Van de Graaff accelerator. The measured densities lie on straight lines passing through the origin. Figure 3 is a compilation of the slopes of these straight-line plots as a function of the gas pressure at which the measurements were obtained. The slopes ( $n_{e0}/i$ ) vary as  $p^{-1}$  at pressures above 0.9 Torr in  $\text{O}_2$  and between 1.5 and 7.0 Torr in  $4\text{N}_2:\text{O}_2$ . Absolute values of ( $n_{e0}/i$ ), referred to the average current density in the cavity, are given in this pressure range by

$$(n_{e0}/i)_{\text{O}_2} = (2.7 \pm 0.6) \times 10^8/p \quad (\text{cm } \mu\text{A})^{-1},$$

$$(n_{e0}/i)_{4\text{N}_2:\text{O}_2} = (4.9 \pm 1.1) \times 10^9/p \quad (\text{cm } \mu\text{A})^{-1}.$$

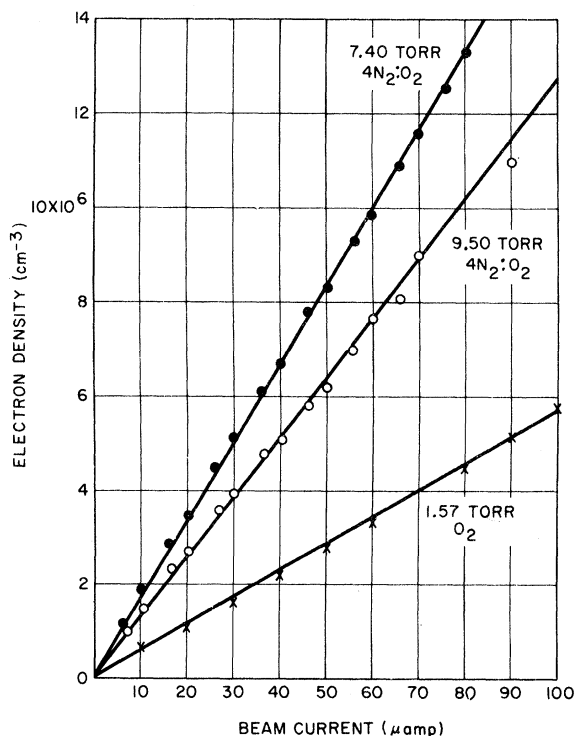


FIG. 2. Typical measurements of electron density as a function of total beam current from Van de Graaff accelerator.

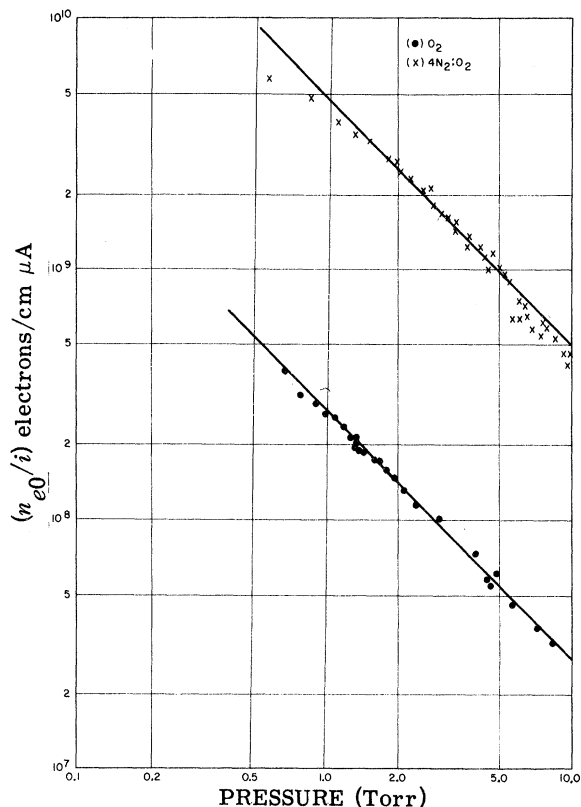


FIG. 3. Steady-state electron density per unit beam current density ( $n_{e0}/i$ ) as a function of gas pressure in O<sub>2</sub> (●) and 4N<sub>2</sub>:O<sub>2</sub> (×).

These include a 20% uncertainty in the absolute beam-flux calibration and a 3% uncertainty in gas-density determination. The behavior of  $n_{e0}/i$  at lower pressures is affected by diffusion and will be described in a future publication.

Time-resolved measurements of electron density were made in the afterglow following the termination of a periodically repeated pulse of beam electrons. Figure 4 shows typical afterglow decays in 4N<sub>2</sub>:O<sub>2</sub> mixtures for a repetitive beam cycle of 5-msec irradiation and 95-msec afterglow. The decays are exponential over at least one decade of density variation. Similar results were obtained for O<sub>2</sub>. In all cases observed, the exponential decay begins directly at the start of the afterglow; that is, extrapolation of the observed exponentially decaying electron density to the beginning of the afterglow yields the measured  $n_{e0}$ . This differs from the behavior observed in the early afterglow of a microwave discharge, in which the occurrence of processes other than the ultimate afterglow decay mode (such as electron cooling, recombination with positive ions, and high-mode diffusion) prevents extrapolation of the late afterglow behavior back into the discharge period. As seen in Fig. 5, the measured exponential decay frequency varies as  $p^2$  in oxygen above 0.9 Torr, and in 4N<sub>2</sub>:O<sub>2</sub> between 1.5 and 7.0 Torr, that is, over the same pressure ranges for which  $n_{e0}/i$  varies as  $p^{-1}$ . At 300°K, the least-squares fits to a  $p^2$  dependence over this pressure range yield the solid lines shown in Fig. 5, which correspond to the electron afterglow removal frequencies

$$\nu_L(\text{O}_2) = (2.12 \pm 0.14) \times 10^{-30} [\text{O}_2]^2 \text{ sec}^{-1},$$

$$\nu_L(4\text{N}_2:\text{O}_2) = (1.10 \pm 0.07) \times 10^{-31} \\ \times ([\text{N}_2] + [\text{O}_2])^2 \text{ sec}^{-1}.$$

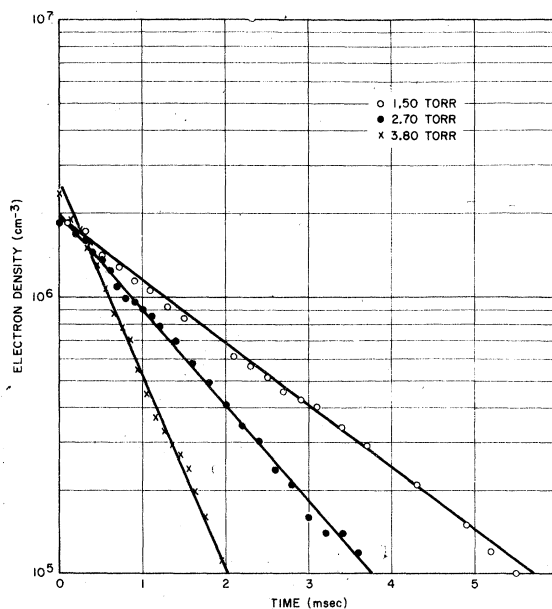


FIG. 4. Typical afterglow decays of electron density in 4N<sub>2</sub>:O<sub>2</sub>.

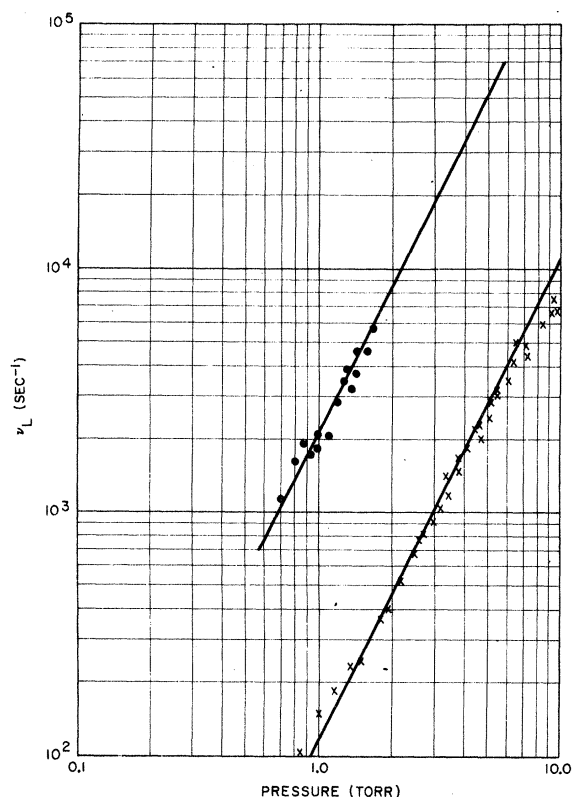


FIG. 5. Electron decay frequency, measured in afterglow, as function of total gas pressure in O<sub>2</sub> (●) and 4N<sub>2</sub>:O<sub>2</sub> (×).

These results include a 3% uncertainty in the determination of gas density and an empirical 6% scatter in the measured decay frequencies. Departures from the  $p^2$  dependence at low pressures result from space-charge limited diffusion of electrons in the presence of both positive and negative ions, to be described in a forthcoming paper. The departure from the  $p^2$  dependence at high pressures in the 4N<sub>2</sub>:O<sub>2</sub> mixture is not yet fully understood. It may be due to electron detachment from negative ions by collisions with O atoms or excited species; its detailed solution will certainly require study of the complex radiation chemistry occurring in air.

If the beam remains on the gas for 50 msec with a 50-msec afterglow,  $\Delta f$  varies in the afterglow as shown by the dashed line in Fig. 6. This differs from the exponential decay observed after the shorter irradiation times by an additive constant frequency shift (10 kHz for the case illustrated), as shown by the solid line in that figure. This apparently constant contribution to  $\Delta f$  arises partly from an ionic component of the plasma conductivity and partly from detachment of electrons from negative ions by beam-generated species. The increased irradiation time in this mode of operation permits the buildup of densities of positive and negative ions on the order of  $10^9 \text{ cm}^{-3}$ , which decay by ionic recombination on a time scale

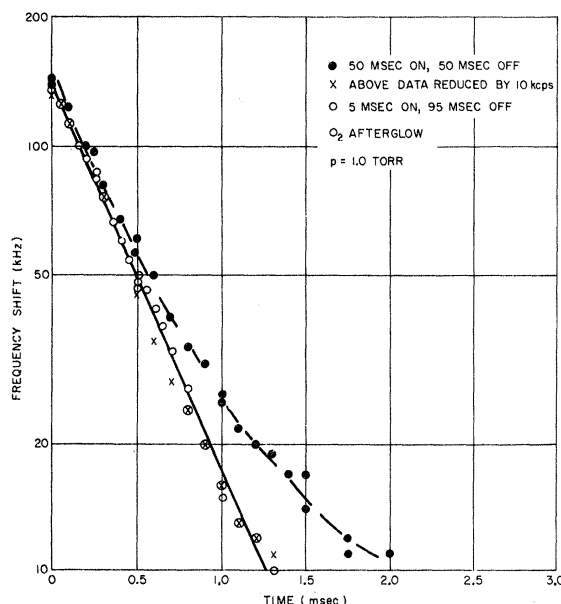


FIG. 6. Duty-cycle effect in O<sub>2</sub> afterglow. Prolonged irradiation (50 msec on, 50 msec off) produces decay shown by (●), shorter beam-on time shown by (○). Subtraction of constant 10 kcps from each solid point yields curve shown by (×), in agreement with (○).

much longer than that of the electron decay. In addition, free atoms and excited species also produced by irradiation can detach electrons from the negative ions to produce a quasi-equilibrium density of free electrons. The ions themselves, together with the detached electrons, can account for the apparently constant contribution to  $\Delta f$  during the electron afterglow.<sup>10</sup>

#### IV. DISCUSSION OF RESULTS

##### A. Afterglow Measurements

At sufficiently high pressures that diffusion may be neglected, and at low ionization so that electron-positive ion recombination is unimportant, the dominant electron removal process for thermal electrons in oxygen and air is expected to be attachment to O<sub>2</sub>.<sup>1,2</sup> This process begins with the formation of an excited negative ion:

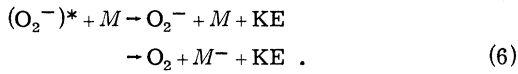


The ion can subsequently be stabilized by one of four possible mechanisms: (a) the electron may autodetach, simply reversing the arrow in Eq. (4); (b) the negative ion may radiate the excess energy as a photon; (c) the ion may dissociate, if this is energetically possible, imparting the excess energy to the kinetic energy of the dissociation fragment in the reaction



or (d) either the excess energy or the excess elec-

tron may be imparted to a third body  $M$  during a collision with the excited ion:



The observation of negative ions in the plasma, as described in the preceding section, makes the occurrence of an attachment process plausible. Also, the observed electron decay frequencies in the afterglow show a quadratic pressure dependence, suggesting the three-body mechanism (4) and (6). Three-body attachment has been observed in electron swarm experiments at low  $E/p$ ,<sup>2</sup> and in the late afterglow of intense pulses of relativistic electron irradiation.<sup>8</sup> In Table I, the rate coefficient  $k_3$  for three-body attachment measured in those studies at 300°K are compared with the results of the present measurement ( $k_3$  is defined by

$$k_3 = \nu_L / [M]^2 , \quad (7)$$

where  $[M]$  is the neutral molecule density). From the observed numerical agreement of the rate coefficients, the dominant electron removal process in the afterglow is identified as three-body attachment of electrons in thermal equilibrium with the gas to neutral O<sub>2</sub> molecules. Any two-body attachment processes which might be present must contribute less than 10% to the lowest observed three-body attachment frequency, giving as upper limits for the two-body rate coefficients

$$k_2(\text{O}_2) \leq 5 \times 10^{-15} \text{ cm}^3/\text{sec},$$

$$k_2(4\text{N}_2 : \text{O}_2) \leq 8 \times 10^{-16} \text{ cm}^3/\text{sec} .$$

### B. Continuous Irradiation Measurements

From Eq. (2), the steady-state electron density during continuous irradiation is equal to  $P/\nu_L \sigma_e$ . There is no *a priori* reason to expect the electron removal process during irradiation, while energetic secondary electrons and various excited species are continually created, to be the same as that in the afterglow, after the electrons have had sufficient time to cool to gas temperature. Nevertheless, in this section it is shown that if the incident electrons satisfy the well-established Bethe formula for energy loss, the steady-state data imply an electron removal process identical with that observed in the afterglow.

An expression has been developed by Bethe<sup>11</sup> for the average rate of energy loss of an electron of initial energy  $E_0$  in traversing a medium of atomic number  $Z$ , atomic mass  $A$ :

$$\begin{aligned} -dE(E_0)/dx &= 2\pi N_A r_0^2 (mc^2/\beta^2) \\ &\times [B_0 - 2 \ln Z + 2 \ln(I/10Z)] \quad (8) \end{aligned}$$

Here  $N_A$  is Avogadro's number,  $r_0$  the classical radius of the electron,  $m$  the electron dynamic mass,  $c$  the velocity of light, and  $\beta c$  the electron velocity.  $B_0$  is a function of  $\tau \equiv (1 - \beta^2)^{-1/2} - 1$  given by

$$\begin{aligned} B_0 &= 21.683 + \ln[\tau^2(\tau + 2)] \\ &- \left(1 + \frac{2\tau + 1}{(\tau + 1)^2}\right) \ln 2 + \frac{1}{(\tau + 1)^2} + \frac{1}{8} \left(\frac{\tau}{\tau + 1}\right)^2 . \quad (9) \end{aligned}$$

$I$ , the mean ionization energy of the medium, is related to the optical oscillator strengths of the target atoms. In general,  $I$  must be evaluated empirically; for accuracy,  $I$  is usually deduced from proton stopping-power experiments. Nelms<sup>12</sup> has computed the electron energy loss predicted by (8) for various materials; the results for 1.5-MeV electrons, in eV/cm of path in O<sub>2</sub>, N<sub>2</sub>, and 4N<sub>2</sub>:O<sub>2</sub> at STP, are shown in Table II. The calculations are in good agreement with the available data on electron stopping.<sup>13</sup>

If all the secondary electrons produced in the primary ionization process are stopped completely in the gas, it has been shown<sup>14,15</sup> that one electron-ion pair is produced for each  $W$  electron volts of energy deposited by the primary electron in the gas.  $W$  is independent of the energy of the primary above several keV, and is a function only of the identity of the target atom. Experimentally determined values<sup>14</sup> for  $W$  are included in Table II for the gases of interest.

From  $-(dE/dx)$  and  $W$  one can evaluate  $S$ , the total number of ion pairs produced per cm of path at STP; from this an effective cross section  $\sigma_e(E)$  for ionization by the primaries and all resulting secondaries (the condition under which  $W$  has been measured) can be defined formally by the relation

$$\sigma_e(E) = 3.72 \times 10^{-20} S . \quad (10)$$

For convenience in the laboratory, the ionization rate is written

$$P = K p i \equiv [2.21 \times 10^{29} (273/T) \sigma_e(E)] p i , \quad (11)$$

where  $p$  is gas pressure in Torr,  $i$  is the electron beam flux in  $\mu\text{A}/\text{cm}^2$ , and  $T$  is the absolute temperature. Predicted values of  $\sigma_e(E)$  and  $K$  are included in Table II.

By using the tabulated values for  $K$  in O<sub>2</sub> and

TABLE I. Comparison of rate coefficients for three-body attachment in O<sub>2</sub> and 4N<sub>2</sub>: O<sub>2</sub> at 300°K ( $k_3$  in units of cm<sup>6</sup>/sec).

	Present work	Drift tube <sup>2</sup>	Intense radiation afterglow <sup>8</sup>
$k_3(\text{O}_2)$	$(2.12 \pm 0.14) \times 10^{-30}$	$(2.0 \pm 0.2) \times 10^{-30}$	$(2.1 \pm 0.1) \times 10^{-30}$
$k_3(4\text{N}_2 : \text{O}_2)$	$(1.10 \pm 0.07) \times 10^{-31}$	$(1.0 \pm 0.1) \times 10^{-31}$	$(1.0 \pm 0.1) \times 10^{-31}$

TABLE II. Computed energy loss and ionization rates for 1.5-MeV electrons in atmospheric gases.

Gas	$-(dE/dx)_{\text{STP}}$ (eV/cm)	$W$ (eV/ion pair)	$\sigma_e(E)$ ( $10^{-18}$ cm <sup>2</sup> )	$K$ ( $10^{11}$ cm sec Torr $\mu$ A) <sup>-1</sup>
N <sub>2</sub>	2140	35.0	2.35	4.75
O <sub>2</sub>	2350	30.9	2.83	5.70
4N <sub>2</sub> :O <sub>2</sub>	2180	33.9	2.45	4.93

4N<sub>2</sub>:O<sub>2</sub>, the measured values of  $n_{e0}/i$ , and Eqs. (2) and (11), one can now determine  $\nu_{L0}$ , the electron-loss frequency effective during continuous ionization. The results are shown in Table III, where  $\nu_{L0}$  is compared with  $\nu_L$  determined from the afterglow decays. The agreement between the rates for the two electron removal processes, which is well within the experimental uncertainties, implies that three-body attachment of thermal electrons at 300°K is the dominant electron-loss process both during continuous irradiation and in the afterglow. This observation is also consistent with the smooth transition from in-beam to afterglow behavior of the electron density which has been described above.

For  $\nu_{L0}$  to be equal to  $\nu_L$ , it is necessary that the energetic secondaries produced by the beam cool to gas temperatures in a time significantly shorter than  $\nu_{L0}^{-1}$ . Thus in O<sub>2</sub> at 1 Torr, the cooling time must be much less than  $5 \times 10^{-4}$  sec. This is in general agreement with recent calculations for air,<sup>16</sup> which give times of the order of 25  $\mu$ sec for electrons with initial energies of tens of eV to cool to gas temperature at 1 Torr.

The above treatment also provides an additional experimental verification of the validity of the Bethe energy-loss formalism. The effective cross-sections for ionization by primaries and all resulting secondaries are therefore taken to be equal to the computed  $\sigma_e(E)$  tabulated in Table II, to within the 25% accuracy of the in-beam measurements.

The ratio of the cross section for total ionization  $\sigma_e(E)$  to that for ionization by the primaries alone,  $\sigma_p(E)$ , is of interest to the ionospheric physicist. In principle, this ratio could be measured in the present experiment by reducing the gas pressure in the chamber until the gas is a thin target for the secondaries. At the required low pressures, however, the dominant electron removal process is space-charge limited diffusion, which changes its characteristics as the ionic composition of the plasma changes with pressure. The results of low-pressure experiments, which

will be presented in a future publication, are therefore difficult to interpret unequivocally at this time in terms of a production coefficient. A direct measurement of primary-ionization cross sections for electrons in the MeV range has recently been made, however, using a technique first developed by McClure,<sup>17</sup> in which the absolute efficiency of a Geiger-Mueller counter is determined as a function of electron energy. Rieke and Prepejchal<sup>18</sup> have obtained primary electron-ionization cross sections which agree with the energy dependence predicted by the Bethe-Born theory of primary ionization.<sup>19</sup> Their results are presented in Table IV for 1.5-MeV electrons; from the table the ratio  $\sigma_e(E)/\sigma_p(E)$  is  $3.0 \pm 0.8$  in agreement with the original prediction of Bethe<sup>19</sup> for air.<sup>20</sup> This is twice the assumed ratio of 1.5, based on a calculation for atomic hydrogen, which is in current usage by ionospheric physicists.<sup>21</sup> The assumption of a ratio  $\sigma_e/\sigma_p = 1.5$  leads to a 50% error in the estimate of the flux of primary electrons during an ionospheric event, if that estimate is based on a total electron effect such as ionization.

## V. SUMMARY

Measurements of electron production and loss rates have been made in oxygen and airlike mixtures of 4N<sub>2</sub>:O<sub>2</sub> for continuous and intermittent irradiation by 1.5-MeV electrons. At pressures between 1 and 10 Torr, the dominant electron removal process is three-body attachment of thermal electrons to O<sub>2</sub> molecules, with rate coefficients characteristic of 300°K both during irradiation and in the afterglow. Ionization rates are consistent with the Bethe theory of electron energy loss in gases, and with measured values of  $W$ , the required energy expenditure by a primary electron to produce an electron-ion pair when all secondaries are stopped in the gas. The ratio of total ionization to that produced by the primaries alone is  $3.0 \pm 0.8$ .

TABLE III. Electron-loss frequency during steady-state irradiation and in the afterglow.

Gas	$\nu_{L0}(\text{steady state})$ (sec <sup>-1</sup> )	$\nu_L(\text{afterglow})$ (sec <sup>-1</sup> )
O <sub>2</sub>	$(2.11 \pm 0.5) \times 10^{-30} [\text{O}_2]^2$	$(2.12 \pm 0.14) \times 10^{-30} [\text{O}_2]^2$
4N <sub>2</sub> :O <sub>2</sub>	$(1.00 \pm 0.25) \times 10^{-31} ([\text{N}_2] + [\text{O}_2])^2$	$(1.10 \pm 0.07) \times 10^{-31} ([\text{N}_2] + [\text{O}_2])^2$

TABLE IV. Primary and total ionization cross sections for 1.5-MeV electrons.

Gas	$\sigma_p(1.5 \text{ MeV}) (10^{-19} \text{ cm}^2)$ G-M efficiency measurement	$\sigma_e(1.5 \text{ MeV}) (10^{-18} \text{ cm}^2)$ Computed and verified in present work	$\sigma_e/\sigma_p$
N <sub>2</sub>	8.35 ± 0.32	2.35 ± 0.6	2.8 ± 0.7
O <sub>2</sub>	9.05 ± 0.21	2.83 ± 0.7	3.1 ± 0.8
4N <sub>2</sub> : O <sub>2</sub>	8.49 ± 0.30	2.45 ± 0.7	2.9 ± 0.7

## ACKNOWLEDGMENTS

The authors wish to express their gratitude to Professor Benjamin Bederson of New York University for his invaluable assistance during the course of this work. For the initial concept of the experiment we are indebted to Dr. Walter G.

Chesnut of the Stanford Research Institute and Professor Sidney Borowitz of New York University. Special thanks are due to Gordon C. Dewey for his continued technical guidance, and to David R. Maerz and Alexander S. Walker, Jr., who assisted in the construction and maintenance of the apparatus.

\*Work supported by the Defense Atomic Support Agency, partly through the U. S. Army Electronics Command, Fort Monmouth, N. J.

†Present address: Department of Physics, City University of New York.

<sup>1</sup>L. M. Chanin, A. V. Phelps, and M. A. Biondi, *Phys. Rev.* **128**, 219 (1962).

<sup>2</sup>J. L. Pack and A. V. Phelps, *J. Chem. Phys.* **44**, 1870 (1966).

<sup>3</sup>B. G. Young, A. W. Johnson, and J. A. Carruthers, *Can. J. Phys.* **41**, 625 (1963).

<sup>4</sup>F. C. Fehsenfeld, A. L. Schmeltekopf, P. D. Goldan, H. I. Schiff, and E. E. Ferguson, *J. Chem. Phys.* **44**, 4087 (1966).

<sup>5</sup>M. A. Biondi, *Phys. Rev.* **84**, 1072 (1951).

<sup>6</sup>M. J. Mulcahy, M. C. Sexton, and J. L. Lennon, in *Proceedings of the Fifth International Conference on Physics of Ionized Phenomena in Gases* (North-Holland Publishing Co., Amsterdam, 1962).

<sup>7</sup>P. J. Chantry, J. S. Wharmby, and J. B. Hasted, *ibid.*

<sup>8</sup>V. A. J. van Lint, J. Parez, D. Trueblood, and M. E. Wyatt, *Rev. Sci. Instr.* **36**, 521 (1965).

<sup>9</sup>M. N. Hirsh, P. N. Eisner, and J. A. Slevin, *Rev. Sci. Instr.* **39**, 1547 (1968).

<sup>10</sup>This interpretation has been substantiated by recent direct mass spectrometric observations of the long-lived positive and negative ions, and by low-frequency impedance measurements of the ion densities; those results, obtained in this laboratory, will be presented in a forthcoming publication.

<sup>11</sup>H. Bethe, *Handbuch der Physik* (Julius Springer, Berlin, 1933), Vol. 24, p. 273.

<sup>12</sup>A. T. Nelms, Natl. Bur. Stand. (U. S.) Circular No. 577, 1957 (unpublished).

<sup>13</sup>See, for example, T. Westermark, *Arkiv Kemi* **17**, 101 (1961); B. Ziegler, *Z. Physik* **151**, 556 (1958); W. Paul and H. Reich, *Z. Physik* **127**, 429 (1950); F. L. Hereford, *Phys. Rev.* **74**, 574 (1948).

<sup>14</sup>W. P. Jesse, *Phys. Rev.* **109**, 2002 (1958).

<sup>15</sup>J. M. Valentine and S. C. Curran, *Rept. Progr. Phys.* **21**, 1 (1958).

<sup>16</sup>A. G. Engelhardt, *Bull. Am. Phys. Soc.* **12**, 231 (1966).

<sup>17</sup>G. W. McClure, *Phys. Rev.* **90**, 796 (1953).

<sup>18</sup>F. F. Rieke and W. Prepejchal, Argonne National Laboratory Rad. Phys. Div. Annual Report ANL-7360, 1966 (unpublished).

<sup>19</sup>H. Bethe, *Ann. Physik* **5**, 325 (1930).

<sup>20</sup>We have recently made preliminary measurements of the effective cross section for excitation of the first negative (0, 0) band of N<sub>2</sub><sup>+</sup> by impact of 1.5-MeV electrons and all resulting secondaries on ground-state N<sub>2</sub>. Our results are roughly a factor of 3 higher than the corresponding cross sections for excitation by primary electrons alone [cf. B. N. Srivastava and I. M. Mirza, *Bull. Am. Phys. Soc.* **13**, 896 (1968); R. F. Holland, *ibid.* p. 897]. The primary excitation measurements, performed at low energies, were scaled to 1.5 MeV by the relativistic Born approximation for the comparison. The ratio of total to primary ionization into a specified final state (N<sub>2</sub><sup>+</sup> B<sup>2</sup>Σ) is thus the same as observed here for gross ionization.

<sup>21</sup>R. E. Meyerott, R. K. M. Landshoff, and J. Magee, Lockheed Missile Systems Division, Sunnyvale, California, Report No. LSMD-48361, 1958 (unpublished).

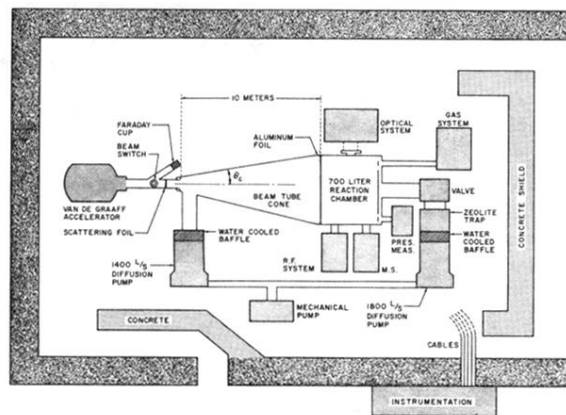


FIG. 1. Schematic diagram of experimental system. The optical and mass spectrometer (M. S.) systems were not employed for the work described in this paper.